PERGAMON

International Journal of Solids and Structures 37 (2000) 1679–1699

INTERNATIONAL JOURNAL OF SOLIDS and STRUCTURES

www.elsevier.com/locate/ijsolstr

High-strain-rate pressure-shear recovery: a new experimental technique

D. Jia, A.M. Lennon, K.T. Ramesh*

Laboratory for Impact Dynamics and Rheology, Department of Mechanical Engineering, The Johns Hopkins University, Baltimore, MD 21218, USA

Received 12 December 1997; in revised form 14 August 1998

Abstract

A new experimental technique is presented that allows for the recovery of a sample that has been subjected to a single well-characterized high-rate shear loading and a single well-characterized longitudinal pulse within a pressure-shear plate impact configuration. Pressure-shear plate impact experiments are traditionally used to investigate the behavior of materials under conditions of very high rate (10^5–10^6 s^{-1}) simple shearing under high hydrostatic pressures. The new technique—known as High-Strain-Rate Pressure-Shear Recovery or HSRPSR—is valuable for the investigation of microstructural influences on the plastic flow of materials under these conditions. Several successful experiments have been performed at strain rates of 10^5 s^{-1} using the HSRPSR technique. The recovered specimens are compared with specimens obtained after deformation within conventional pressure-shear plate impact experiments. As an example of the utility of this recovery technique, the paper presents the microstructural characterization of specimens of α-titanium after deformation at strain rates of 10^5 s^{-1} and under superimposed hydrostatic pressures of several GPa.

Keywords: Pressure-shear plate impact; Recovery; Dynamic behavior; High strain rate; Microstructural evolution

1. Introduction and background

A number of experimental approaches have been developed for investigation of the high-strain-rate behavior of materials. These include the compression Kolsky bar or split-Hopkinson pressure bar (Kolsky, 1949), and modifications of the latter technique known as the torsion Kolsky bar (Duffy et al., 1971) and the tension Kolsky bar (e.g. Chichili and Ramesh, 1995) which allow the development of other stress states. The strain rate range attainable with Kolsky bars is 10^2–10^4 s^{-1}. The technique most

* Corresponding author. Tel.: 001-410-516-7735; fax: 001-410-516-7254.
E-mail address: ramesh@jhu.edu (K.T. Ramesh)

0020-7683/00/$ - see front matter
PII: S0020-7683(98)00278-9

commonly used for obtaining stress-strain curves at higher strain rates is the high-strain-rate pressure-shear (HSRPS) plate impact technique (Clifton and Klopp, 1985; Yadav and Ramesh, 1995) which can develop shear rates of 10^4–10^6 s^{-1} under superimposed compressive stresses of several GPa. When these techniques are combined with the more traditional servohydraulic testing approaches at lower (10^{-6} –10^0 s^{-1}) strain rates a complete description of the rate-dependent mechanical response of a material becomes possible (Yadav et al., 1995; Chichili et al., 1997).

Through such approaches, a large number of materials (especially metals) have been shown to develop substantially higher flow stresses at high rate of deformation. A fundamental understanding of this material behavior at high strain rates requires an understanding of the microscopic mechanisms that are active during dynamic deformations, and consequently of the evolution of microstructure with loading. An understanding of these mechanisms would allow for the design of materials with the desired behavior at high strain rates (high strain rates are developed within a number of manufacturing and machining processes, and in armor/anti-armor interactions). However, characterizing the evolution of microstructure at high strain rates requires a different experimental capability, that of recovering specimens of the material after they have been subjected to a well-characterized high-rate loading. Thus, controlled dynamic experiments (also called dynamic recovery experiments) are essential for understanding the evolution of microstructure with the loading history. Various methods have been developed to recover samples in the compression Kolsky bar (da Silva and Ramesh, 1997; Nemat-Nasser et al., 1991). Microstructural characterization of specimens recovered using these techniques, in conjunction with specimens recovered from servohydraulic testing at lower rates, has led to substantial improvement in understanding of material behavior at rates as high as 10^4 s^{-1} (Chichili et al., 1997; Follansbee and Gray, 1989). However, an equivalent high-strain-rate recovery capability has not been available, until now, at strain rates above 10^4 s^{-1}. Since the strongest rate sensitivity of materials is often observed at these higher rates, this lack of capability has constrained the development of rational mechanism-based models for the high-strain-rate behavior of materials.

Models for the rate-dependent inelastic deformation of solids (e.g. the Johnson-Cook model) often represent empirical fits to data and are not related to the evolving microstructure. Such empirical models are unable to capture second derivatives, such as the dependence of the strain hardening on strain rate, and are unable to account for evolving microstructural effects such as the influence of prior loading (at a different strain rate or temperature) on the current strength. A number of more recent models attempt to incorporate microstructural information into the constitutive description by choosing functional forms that correspond to specific microscopic deformation mechanisms (Mecking and Kocks, 1981; Zerilli and Armstrong, 1987). Current versions of all of these models are typically unable to capture the very high rate ($> 10^4$ s^{-1}) response of materials because of an insufficient understanding of the microstructural mechanisms active at these very high strain rates. The ability to recover and then characterize the microstructure of specimens that have been subjected to controlled deformations at very high strain rates ($> 10^4$ s^{-1}) is therefore of great interest.

The high-strain-rate pressure-shear (HSRPS) plate impact technique (Clifton and Klopp, 1985; Yadav and Ramesh, 1995) is able to develop very high shear rates (10^4–10^6 s^{-1}). However, accurate correlation of the micromechanisms of deformation with the recorded loading history is not possible in these experiments because the specimen experiences repeated passages of the longitudinal and transverse pulses due to reflections from the flyer and anvil plate surfaces. In addition, the specimen may be severely damaged in the high energy collision between the projectile and catcher. It is therefore necessary to modify this technique to enable recovery.

A recovery technique for normal plate impact was developed by Kumar and Clifton (1979) for the study of dislocation mobility in lithium fluoride. In this approach a momentum trap mounted behind the specimen is designed to absorb the momentum from the flyer, and a specially designed specimen holder reduces the projectile velocity to zero immediately after impact. The technique ensures that the

microstructural changes in the specimen result only from the initial compression pulse and not from reverberations of the pulse or additional deformation caused by the projectile reloading, and is thus a true recovery technique (although it is associated with compressive wave propagation rather than homogeneous high-rate loading). However, the approach of Kumar and Clifton cannot be applied directly to the pressure-shear plate impact case, because both longitudinal and transverse waves in the flyer plates must be trapped if the specimen is to be subjected to a well-characterized loading pulse. Because transverse (shear) waves travel more slowly than longitudinal waves, a simple momentum trap configuration may leave behind a portion of the transverse pulse.

Two distinct types of pressure-shear plate impact recovery experiments can be designed, each with distinct applications:

(i) Single Wave Pressure-shear Recovery (SWPSR), and
(ii) High-Strain-Rate Pressure-shear Recovery (HSRPSR).

The goal of the first kind of experiment (single wave pressure-shear recovery or SWPSR) is to compress the specimen with a normal compression wave and apply shear with a single transverse shear wave, and then to recover the specimen without further loading. This is of great value in studying the effects of large amplitude wave propagation and in studying damage modes in materials. The goal of the second kind of experiment (high-strain-rate pressure-shear recovery or HSRPSR) is to recover a specimen that has been subjected to a single well-characterized homogeneous deformation at high strain rates ($>10^4$ s^{-1}). This is the best approach to studying the microscopic deformation mechanisms that are active at very high strain rates, and this information can then be more easily fed back into constitutive models for material behavior at high strain rates. This paper describes an experimental technique of the second kind and provides an example of the application of the technique. A very brief description of the SWPSR technique is provided in the next paragraph for completeness.

In single wave pressure-shear recovery (SWPSR), all of the flyer and target plates are impedance matched. A single wave pressure-shear recovery technique was developed by Yadav et al. (1993) for examining the development of damage in an alumina/aluminum composite. A similar configuration was used by Machcha and Nemat-Nasser (1994) to study alumina ceramic specimens. In this technique, a stationary target assembly consisting of a thin specimen, anvil plate and an impedance-matched momentum trap is impacted by a sandwich consisting of two hard plates separated by a 'shear trap' composed of a very thin polymeric layer (Yadav et al. 1993) or a thin lubricant layer (Machcha and Nemat-Nasser, 1994). However, this technique is very time consuming and expensive due to the large number of plates required for the flyer and target assemblies.

This paper describes the newly developed high-strain-rate pressure-shear recovery technique, presents some experimental results using the technique, and compares the results of the new recovery technique with the results of the conventional (non-recovery) pressure-shear configuration. The conventional high-strain-rate pressure-shear plate impact technique is first described briefly to establish some of the fundamental characteristics of such very-high-rate experiments. The new recovery technique is then easily described as a modification of the conventional technique. The paper concludes by presenting the application of the technique to the examination of deformation twinning in α-titanium at very high strain rates.

2. Conventional high-strain-rate pressure-shear plate impact experiments

The conventional high-strain-rate pressure-shear plate impact technique was developed specifically for the study of the shearing behavior of materials undergoing homogeneous shearing deformations at extremely high shear rates while under superimposed hydrostatic pressures—a more detailed description

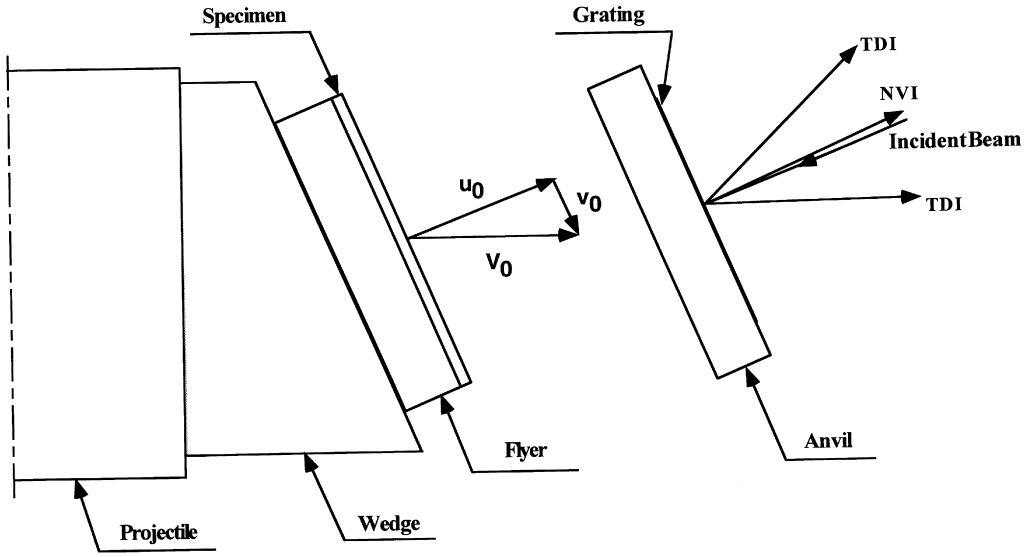

Fig. 1. Experimental configuration for the conventional high-strain-rate pressure-shear plate impact experiment. Projectile velocity V_0 is determined just before impact using the laser line velocity sensor, and particle displacement and particle velocity measurements are made at the center of the rear surface of the anvil plate using laser interferometry.

of this technique is provided by Clifton and Klopp (1985) and a description of the specific implementation of the technique used here is provided by Yadav and Ramesh (1995). The experiment involves the impact of plates that are flat and parallel but inclined relative to their direction of approach (Fig. 1). The specimen used is a thin ($\sim$100 μm) plate carried on a hard elastic plate (the 'flyer'); the flyer is carried on a projectile which is launched down the barrel of a gas gun (with velocity V_0) towards a stationary target plate (sometimes called the 'anvil'). The flyer and the target plates are aligned before impact using an optical technique developed by Kumar and Clifton (1979). At impact, plane longitudinal (compressive) and transverse (shear) waves are generated in both the specimen and the anvil plates due to the angle between the direction of projectile motion and the surface normals of the plates. These waves reverberate within the specimen, remaining loading waves since the impedance of the material of the flyer and target plates is (by design) higher than that of the specimen material. Due to the finite compressibility of the specimen, the normal stress in the specimen attains an equilibrium value. Measurements of the normal and transverse particle velocities at the free surface of the anvil plate are made using laser interferometry off a diffraction grating (typically 200 lines mm^{-1}) that is photo-deposited onto the rear surface. The experiments are so designed that the target and flyer plates remain elastic. Hence, the information on the stress levels sustained by the specimen material can be obtained by measuring particle velocities in the target plate. The entire experiment is completed before any unloading waves from the periphery of the plates arrive at the point of observation, so that only plane waves are involved and a one-dimensional analysis can be used.

Normal particle velocity and transverse particle displacement of the rear surface of the anvil plate are detected at the same point (at the center of the rear surface) by a Normal Velocity Interferometer (NVI), shown in Fig. 2, and a Transverse Displacement Interferometer (TDI), shown in Fig. 3. This latter interferometric technique was developed by Kim and Clifton (1977). The projectile velocity is measured (just before impact occurs) using a laser line velocity sensor (LLVS, shown in Fig. 4) developed by Ramesh and Kelkar (1995). Projectile velocities approaching 300 m s^{-1} can be achieved in this laboratory.

These experiments can be analyzed using a one-dimensional elastic stress wave analysis (Clifton and

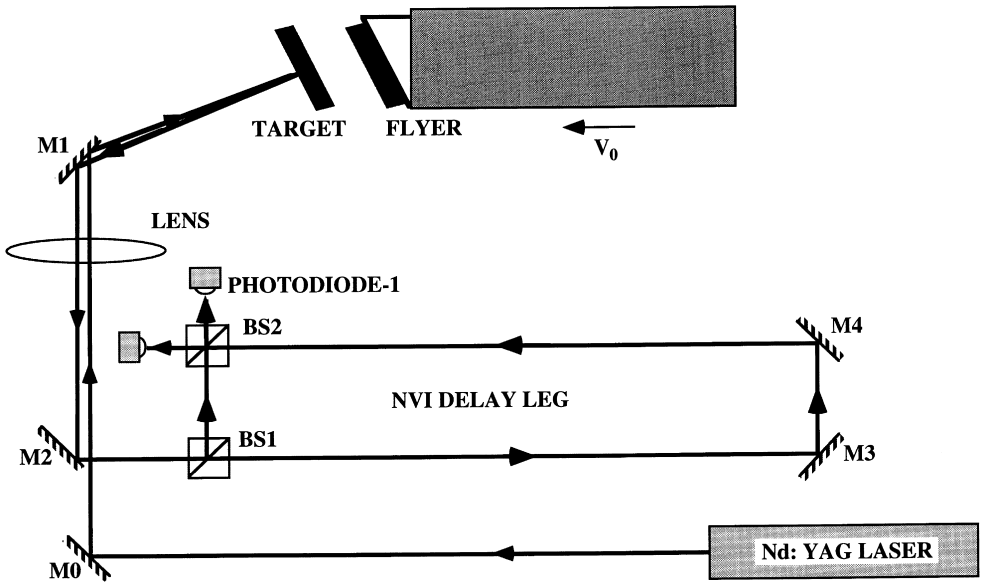

Fig. 2. Normal Velocity Interferometer (NVI). The reflected beam is split at beamsplitter BS1 and recombined at BS2 after one component has traversed a delay leg. The resolution of the interferometer is controlled by the time delay introduced by the delay leg.

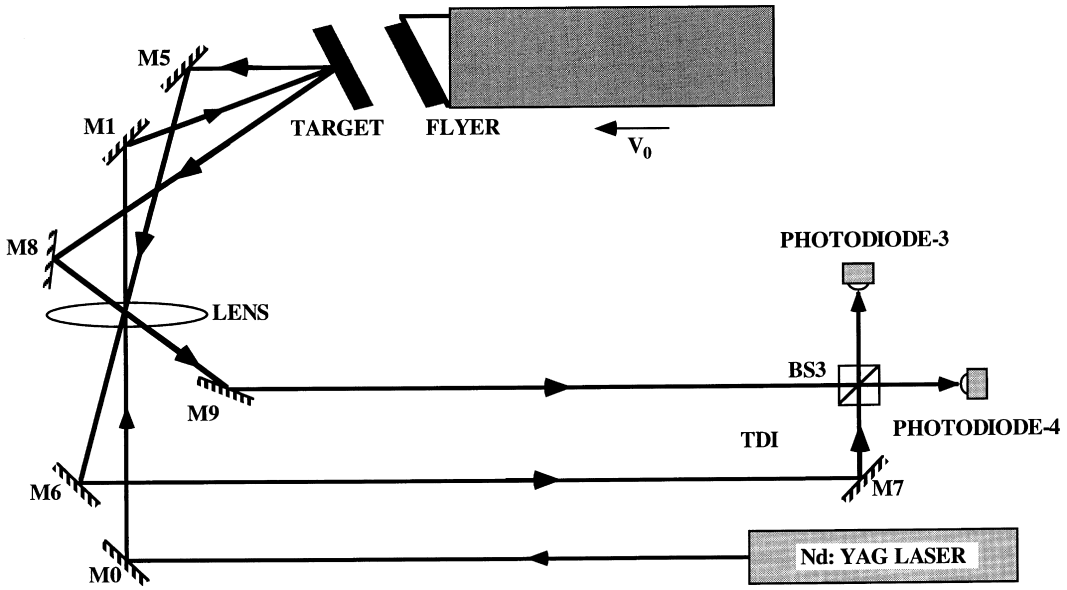

Fig. 3. Transverse Displacement Interferometer (TDI). A diffraction grating deposited on the target diffracts the incident beam at discrete angles. Combining two nth-order diffracted beams at BS3 results in a phase-shift due to transverse particle displacement at the rear surface of the target.

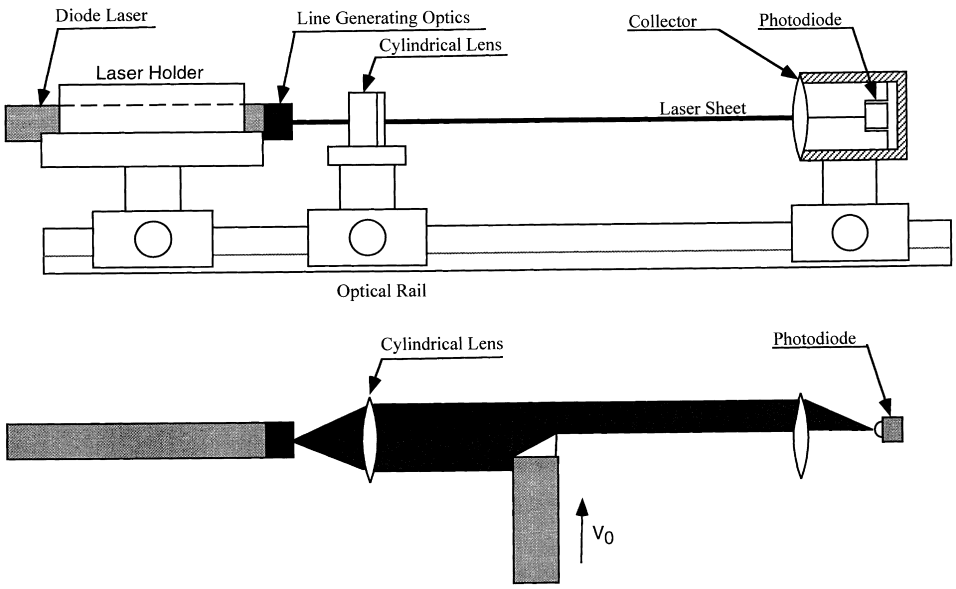

Fig. 4. Laser Line Velocity Sensor (LLVS). The moving projectile blocks off part of the light as it crosses the laser sheet; the projectile velocity and acceleration can be determined by measuring the integrated light at the photodiode using the known (uniform) intensity of the laser source.

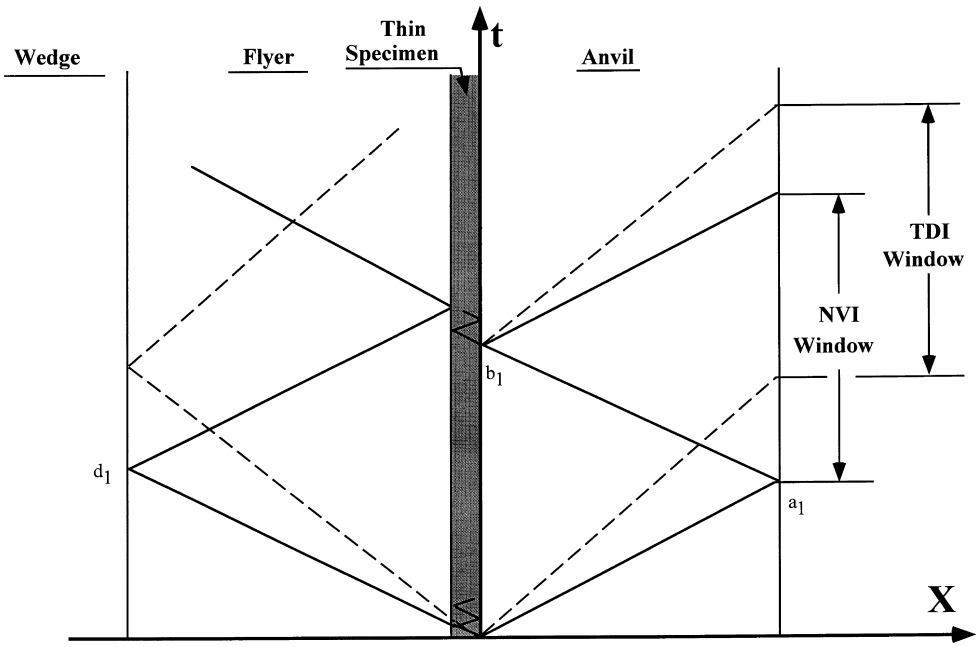

Fig. 5. Time–distance (Lagrangian) diagram of the wave propagation during a conventional high-strain-rate pressure-shear plate impact experiment.

Klopp, 1985) because the waves generated by the planar impact are plane waves (until unloading waves from the target periphery reach the point of observation). Fig. 5 is a time–distance diagram that shows the wave propagation during such an experiment. When the impact occurs, a normal compression wave and a shear wave are generated at the impact surface of the anvil plate and the specimen/flyer assembly (solid lines denote normal waves and dashed lines denote shear waves in Fig. 5). When the normal wave in the anvil reaches the rear surface (at time a_1) the compression wave reflects as a tension wave which propagates back into the anvil plate, unloading the compression in the anvil. When this reflected normal wave reaches the impact surface (at time b_1), the normal stress in the specimen is unloaded; this typically results in an effective unloading of the shear in the specimen as well, since the specimen/anvil interface is likely to slip without a superimposed compression. Since the anvil remains elastic, there is a linear relationship between the stresses and the particle velocities in the target plate. Hence, it is sufficient to measure the normal and transverse particle velocities in the target plate to deduce the stress state and deformation state within the specimen. Thus information on the compressive state of the specimen is obtained using the normal velocity interferometer within the time denoted 'NVI Window' in Fig. 5 and information on the shearing of the specimen is obtained using the transverse displacement interferometer within the region denoted 'TDI Window'.

Once sufficient reverberations of the normal stress have occurred, the normal compressive stress is given by:

$$\sigma_n = \frac{1}{2}\rho c_1 V_0 \cos\theta, \tag{1}$$

where ρc_1 is the acoustic impedance of the target plate material, V_0 is the projectile velocity and θ is the skew angle (using simple elastic wave theory). The hydrostatic pressure in the specimen can be approximated to the normal compressive stress (Ramesh and Clifton, 1992), being less than σ_n by a magnitude approximately equal to the flow stress sustained (assuming J_2-flow plasticity). The shear stress in the specimen also increases with each reverberation of the shear wave within the specimen, until the specimen starts flowing at a stress level τ. Thereafter, a finite difference in the transverse velocity can be maintained across the two surfaces of the specimen. The nominal shear strain rate in the specimen is then given as:

$$\dot{\gamma} = \frac{V_0 \sin\theta - v_{\mathrm{fs}}}{h}, \tag{2}$$

where v_{fs} is the transverse particle velocity measured at the rear surface of the target and h is the specimen thickness. The nominal shear strain rate in the specimen can be integrated to give the nominal strain history in the specimen:

$$\gamma(t) = \int_0^t \dot{\gamma}(\tau)\,\mathrm{d}\tau. \tag{3}$$

The shear stress history in the specimen is obtained from the transverse particle velocity history using the elastic characteristics of the target plate:

$$\tau(t) = \frac{1}{2}\rho c_{\mathrm{s}} v_{\mathrm{fs}}(t), \tag{4}$$

where ρc_{s} is the shear impedance of the target plate material. The shear stress and the shear strain in the specimen can now be cross-correlated to give the shear stress vs shear strain curve for the material tested at an essentially constant shear rate corresponding to eqn (2). The technique is thus able to

provide a stress–strain curve for the material at high shear rate under a superimposed high compressive stress.

In terms of characterization of deformation micromechanisms, however, there remain normal waves and shear waves propagating in the specimen/flyer because the flyer is typically thicker than the anvil in this configuration. These residual waves can further deform the specimen at times after the NVI and TDI information windows shown in the figure. In addition to the residual wave propagation, the moving (and still accelerating) projectile re-accelerates the specimen/flyer into the anvil and catcher and causes further damage. Thus the technique does not generally permit recovery of the specimen except under certain fortuitous conditions.

3. High-strain-rate pressure-shear recovery: a new experimental technique

The final objective of a recovery experiment is an analysis of the deformation microstructures of a specimen material due to some known loading conditions. By this definition, nearly all quasistatic experiments can be thought of as recovery experiments. After being subjected to a low rate tensile or compressive loading, during which stresses and strains are recorded, the specimen is removed and sectioned for microstructural analysis. When conducting dynamic experiments, however, it becomes more difficult to avoid material deformations that occur after the data collection ends. This difficulty arises mainly because large accelerations and velocities must be suddenly applied to accomplish the high strain rate loading. In the case of pressure-shear plate impact, the projectile which carries the flyer assembly must be stopped by ramming into some sort of catching device (a box of lead plates, for instance). This is a high-energy impact which will damage the specimen material in ways that cannot be accounted for when analyzing the deformed microstructure. Similarly, the stress waves that are generated in the impacting plates normally persist longer than the data collection window, causing unmonitored damage in the specimen material. Therefore, the design of a recovery experiment must include elements which allow well-characterized deformations within the loading regime of interest to

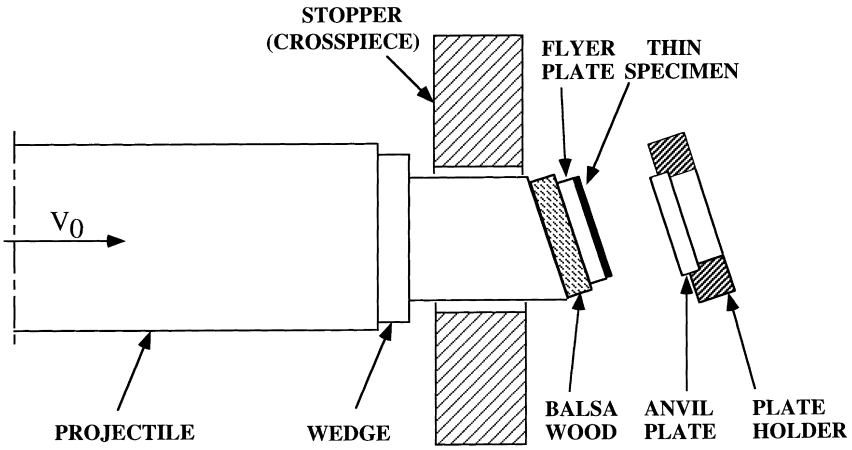

Fig. 6. Experimental configuration for the new High-Strain-Rate Pressure-Shear Recovery (HSRPSR) technique. A strong 'stopper' assembly is used to stop the forward motion of the projectile immediately after the specimen and flyer plates impact the target. The flyer/specimen assembly is mounted on a balsa wood plate to provide a very low-impedance condition at the rear surface of the flyer.

occur, but prevent specimen damage outside of the data collection window due to residual velocities, accelerations, stress waves or anything else which could alter the specimen's microstructure.

The experimental configuration for the new high-strain-rate pressure-shear plate impact recovery technique is presented in Fig. 6. The thin specimen is carried on a flyer, as in the conventional pressure-shear experiment; however, the back of the specimen/flyer assembly is glued to a plate of balsa wood (as in the Kumar and Clifton (1979) normal recovery experiment) that provides a low-impedance rear surface for control of the wave reflections. The balsa wood is itself glued to an extended 'wedge', which fits into the projectile and defines the skew angle at which impact occurs. The part of the wedge that fits into the projectile has a flat shoulder machined orthogonal to the projectile axis. Just after the flyer and anvil plates impact, the flat shoulder of the wedge comes into contact with a strong 'stopper' made of heat treated steel so that the kinetic energy of the entire projectile is absorbed by the stopper assembly and the projectile velocity is reduced to zero. The anvil itself is carried within a special holder that allows for the initial alignment of the flyer and anvil plates, and the rear surface of the anvil plate has a diffraction grating photo-fabricated onto the surface for interrogation by the interferometers. The thickness of the balsa wood in the recovery experiments is 3–5 mm (these design parameters are critical to ensure both timely stopping of the projectile and sufficiently small misalignment or tilt at impact).

The stopper assembly has a two-component design (Fig. 7). The main structural component is a heavy, welded steel base which has two vertical supports and a stage for mounting the target plate holder. The base is reinforced to prevent flexing (which would cause motion of the vertical supports) and is heat-treated to remove residual welding stresses as well as to increase the toughness of the metal. The second component of the stopper assembly is a removable crosspiece which is attached to the vertical supports. The crosspiece is designed to transfer the momentum of the projectile to the vertical supports without deflecting significantly. The fact that the crosspiece is a separate component from the base allows for easy alignment of the plates, and also makes the crosspiece a fairly inexpensive, replaceable component. At the center of the crosspiece is a hole which allows the specimen/flyer and the front section of the wedge to pass through.

The wave propagation in the high-strain-rate pressure-shear recovery experiment is presented in the

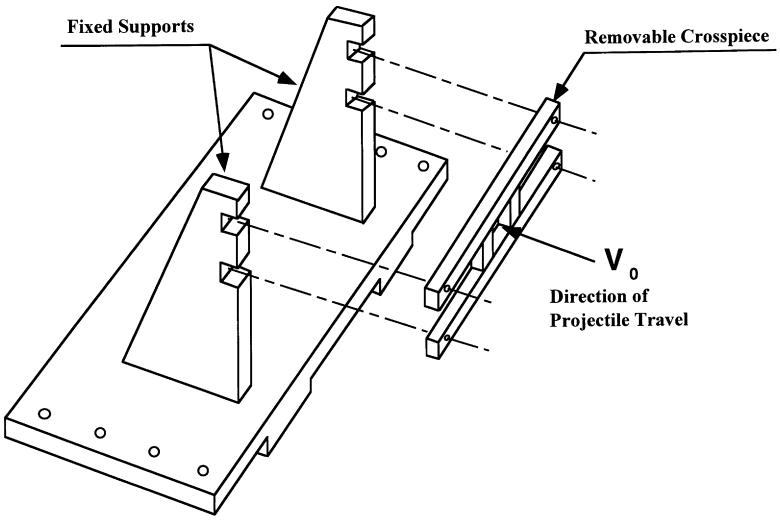

Fig. 7. The stopper assembly for HSRPSR experiments. The actual impact occurs on the cross-piece which is removable to allow for easier alignment. The cross-piece is also designed to be easily replaced if damaged.

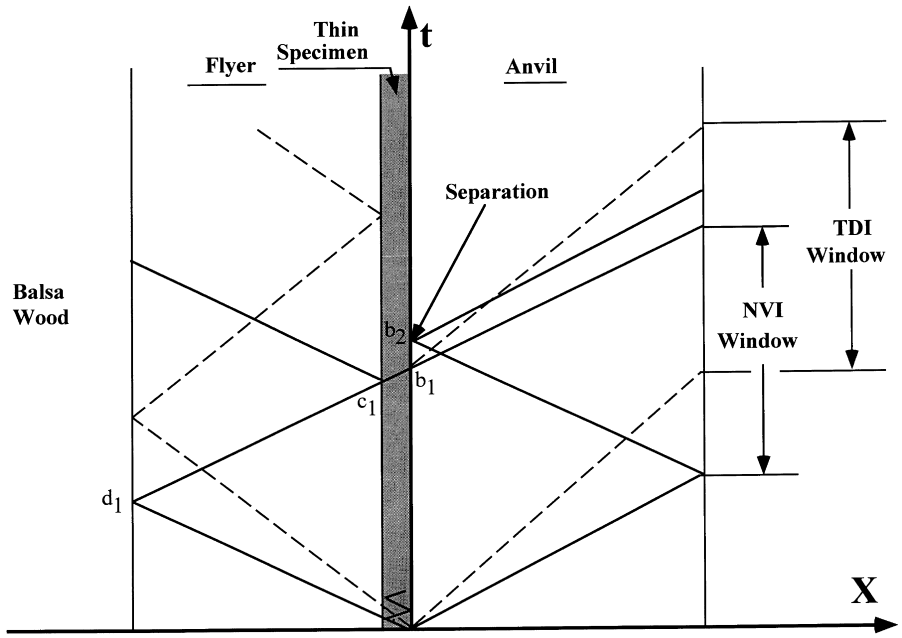

Fig. 8. Time–distance (Lagrangian) diagram of the wave propagation during a High-Strain-Rate Pressure-Shear Recovery experiment. When the normal unloading in the anvil arrives at the specimen interface, the anvil flies away carrying all of the longitudinal pulse with it, as well as a substantial fraction of the shear pulse. The remaining shear pulse in the flyer is unable to reload the specimen plastically.

time–distance diagram of Fig. 8. The overall plate configuration is similar to that in the conventional high-strain-rate pressure-shear experiment, with the distinction that in the new recovery technique the combined thickness of specimen and flyer is less than that of the anvil plate. A second distinction is that the flyer in the recovery experiment is backed by the very low-impedance balsa wood. The immediate consequence of the first distinction is that the normal wave reflected from the back of the flyer plate reaches the specimen (at time c_1) before the normal wave reflected from the rear surface of the anvil plate. The consequence of the second distinction (the low-impedance balsa wood backing) is that the initial compressive longitudinal wave is reflected from the flyer/balsa-wood interface as a tensile unloading wave. This reflected wave thus unloads the compressive stress in the specimen to zero. By proper design of the flyer and anvil thicknesses, the reflected tensile wave from the rear surface of the anvil arrives at the specimen at a later time b_2. This tensile wave is now propagating into an unstressed region and so the wave generates tension at the specimen/anvil interface. Since the specimen/anvil interface cannot support tension, separation occurs between the anvil and the specimen; the anvil flies away towards the catcher at a velocity $V_0 \cos\theta$, carrying within it the entire longitudinal pulse and a significant fraction of the shearing pulse. Thus the anvil itself operates as a momentum trap.

The flyer/specimen assembly is at zero velocity in the normal direction after time b_1 in Fig. 8. A very short time later the moving projectile is brought to rest by the stopper assembly before it can re-accelerate the flyer-specimen assembly. The interval of time before the projectile itself contacts the stopper is determined by the thickness of the balsa wood spacer and the relative dimensions of the stopper and target holder. Photographs showing top and rear views of the entire assembly (including projectile and target holder) are presented in Figs. 9 and 10, respectively. The process through which the projectile is stopped after impact should be clearly evident from these Figures. It is absolutely essential

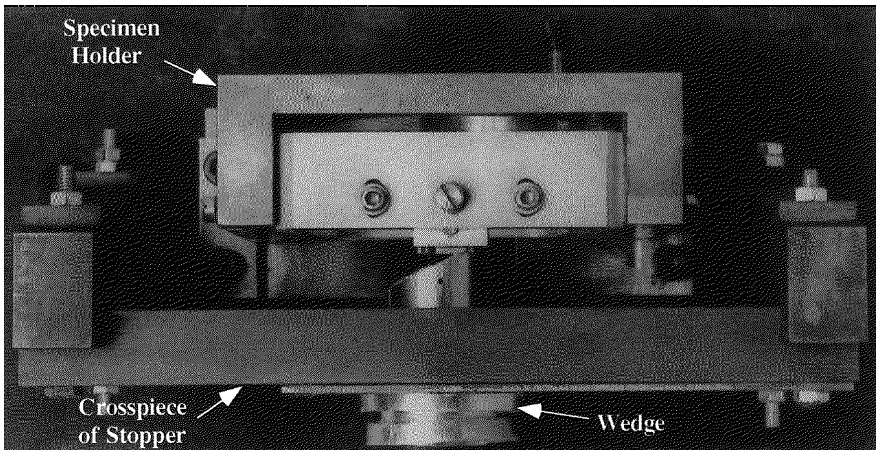

Fig. 9. Photograph of the projectile and stopper assembly (top view). The target plate is not shown.

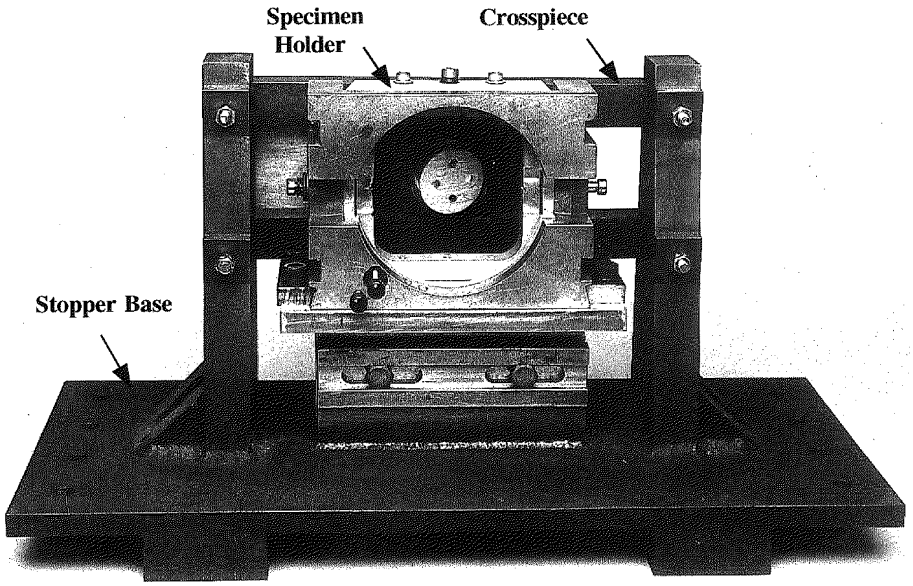

Fig. 10. Photograph of the stopper assembly (rear view, with the projectile velocity coming out of the plane of the paper). The base of the stopper has a stage for setting the height and horizontal position of the specimen holder.

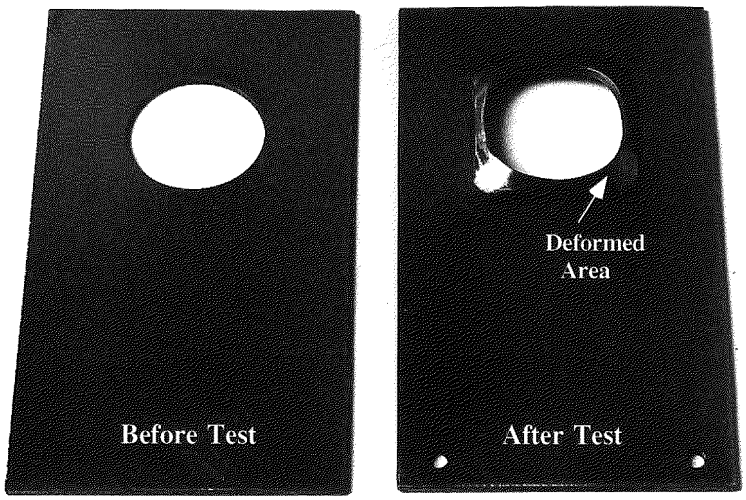

Fig. 11. Sacrificial steel plate attached to the front of the stopper crosspiece, shown before and after impact. By plastically deforming during the projectile impact, the steel plate absorbs some of the energy of the impact and helps to prevent extrusion of the projectile wedge.

that a strong stopper assembly, robust enough to be used repeatedly, is employed for stopping the projectile immediately after the initial plate impact. A disposable steel plate (Fig. 11) with a round hole is used on the front surface of the stopper crosspiece for absorbing and redistributing the kinetic energy of the moving projectile by deforming plastically around the hole.

Returning to the wave propagation diagram of Fig. 8, it is clear that a part of the shear wave still exists in the flyer after the time c_1. However, this shear pulse cannot reload the thin specimen because the specimen/flyer interface will slip because no pressure exists on the interface and simultaneously the other side of the specimen becomes a free surface.

The primary effect of this residual pulse is to impart some residual rigid body velocity to the specimen. The momentum transfer to the anvil and supports is such that at the end of the test the specimen is typically recovered from the target chamber floor.

The high-strain-rate plastic deformation of the material of the specimen occurs through a process identical to that in the conventional high-strain-rate pressure-shear plate impact experiment, and the data acquisition and data reduction procedures are identical to those for such experiments (i.e. using eqns (1)–(4)). The requirements for plane wave loading are also met in the same way. As in the conventional plate impact experiment, radial unloading waves from the peripheries of the plates will pass through all regions of the specimen; however, these waves are too small to cause significant plastic deformation in comparison with the primary loading. Thus the design of the experiment allows for the recovery of the specimen after it has been subjected to a single well-characterized homogeneous high-rate shearing deformation under superimposed compression, with the magnitudes of the shear stresses, shear strain rates and normal stresses determined directly from the outputs of the normal velocity and transverse displacement interferometers using eqns (1)–(4).

The next section presents the results of the HSRPSR tests on α-titanium to demonstrate both the operation and the utility of the new technique.

Table 1
Quasistatic mechanical properties of α-titanium[a]

Young's Modulus [GPa]	Poisson's Ratio	Yield strength [MPa]	Tensile strength [MPa]	Elongation %
105	0.34	337	506	25

[a] Young's Modulus and Poisson's Ratio are mean values taken from the literature, while the other properties listed were supplied by the manufacturer.

4. An application of HSRPSR: high-rate deformation mechanisms in α-titanium

4.1. Materials issues

The material investigated is a commercially pure α-titanium (a hexagonal close-packed metal) obtained from President Titanium Inc. The material had been annealed at 705°C for 2 h and then air cooled, and the resulting microstructure consisted of equiaxed grains with an average grain size of 35 μm. Table 1 lists nominal values for the quasistatic mechanical properties of the material in the as-received condition.

4.2. Rate-dependent response and microstructural evolution

The rate-dependent mechanical behavior of α-titanium has been systematically characterized over a wide range of strain rates (10^{-5}–10^{+5} s^{-1}) using a combination of quasistatic and dynamic testing techniques, including conventional high-strain-rate pressure-shear plate impact, in a previous work (Chichili et al., 1997). Both the flow stress and the degree of strain hardening of the material increase with increasing strain rate, while the flow stress decreases with increasing temperature. Chichili et al. (1997) also performed a number of dynamic recovery experiments (da Silva and Ramesh, 1997) using the compression Kolsky bar and observed that deformation twinning was a prominent feature of the high-rate deformations of this material. The twin density in the deformed microstructure was observed to be a function of the compressive flow stress sustained. However, independent high-rate torsion tests (Chichili, 1997) showed very little evidence of deformation twinning even at similar stress levels. It appears, therefore, that the deformation twinning mechanism varies with the trajectory in stress space (there is independent evidence of this at quasistatic rates, e.g. Yoo, 1981). Thus the newly developed

Table 2
Summary of selected plate impact experiments for α-titanium

Test no.	Thickness [μm]	Velocity [m s^{-1}]	Angle [degrees]	Pressure [GPa]	Shear stress [MPa]	Strain rate [10^5 s^{-1}]
Ti410[a]	122	119	24	2.45	463	1.04
Ti619[a]	122	123	22	2.57	460	0.91
Ti529	125	138	22	2.88	453	1.29
Ti969	118	123	22	2.57	446	0.97

[a] Recovery experiments.

high-strain-rate pressure-shear recovery experiment promises to be of great utility in studying the deformation twinning mechanism.

4.3. HSRPSR experiments on α-titanium

Two high-strain-rate pressure-shear recovery (HSRPSR) plate impact experiments and several conventional high-strain-rate pressure-shear experiments have been performed on this α-titanium at strain rates of $\sim 10^5$ s^{-1}. Table 2 is a summary of a subset of the pressure-shear plate impact experiments.

The material used for the flyer and anvil plates is Carpenter D-3 steel. The plates and specimen are each 25.4 mm (1 inch) in diameter, and the flyer and anvil plates are 2.8 and 3.1 mm thick, respectively. Since the specimens are ~0.120 mm thick, the total thickness of the flyer and the specimen is less than the anvil plate (as necessary to ensure recovery). The ratio of the specimen thickness to the flyer thickness is typically ~0.04. The specimens are made flat (to a half-wavelength of light) and parallel using a special vacuum fixture and a lapping machine. A 200 lines mm^{-1} diffraction grating was deposited on the rear surfaces of the anvil plates in each of the experiments. A catcher tank filled with corrugated lead plates is used to stop the projectile in the conventional pressure-shear tests. Since the stopper assembly brings the projectile to rest in the HSRPSR experiment, a catcher is not needed during a recovery test. However, a catcher tank carrying a foam front plate is used in the target chamber during recovery experiments: the foam both stops the anvil and serves as a 'witness plate' to determine whether any other components develop a substantial residual velocity (this terminology is borrowed from the ballistics community).

The transverse displacement interferometer (TDI) signal obtained during one of the HSRPSR experiments (Test No. Ti619) is presented in Fig. 12 (time zero in this Figure corresponds to the arrival of a trigger signal from the tilt pins used to measure the misalignment or tilt between flyer and anvil plates). The initial arrival of the normal compressive wave at the rear surface of the anvil is clearly evident, as is the arrival of the shear wave (the time when the fringes suddenly appear). The fringes end at a time corresponding to the arrival at the specimen of the normal unloading wave from the flyer/balsa wood interface. Each fringe on this TDI signal corresponds to a 2.5 μm transverse displacement; this data is reduced to obtain the transverse velocity at the rear surface by applying a locally developed algorithm that first corrects for the amplitude variation in the fringes using an envelope technique. Once the transverse free-surface velocity v_{fs} is obtained, a shear stress vs shear strain curve can be computed for the material of the specimen using eqns (2)–(4). For the case of the experiment shown in Fig. 12 the shear strain rate was 0.91×10^5 s^{-1}, and the corresponding superimposed compressive stress was about 2.57 GPa using eqn (1).

Fig. 13 presents the shear stress vs shear strain curve for α-titanium that is obtained by processing the TDI signal (Fig. 12) from this experiment using eqns (2)–(4). The shear stress is observed to increase somewhat at small strains, but the nature of the pressure-shear experiment is such that the small strain data ($<2\%$) should be discounted because of potential wave propagation effects. The material is observed to sustain a fairly high flow stress in shear, on the order of 400 MPa, at this nominal shear rate of 0.91×10^5 s^{-1}. Note that pressure-shear tests are inherently nearly adiabatic, because the total time of the experiment is so short (~1 μs). The stress–strain curve of Fig. 13 is therefore probably affected by the thermal softening of the material (this is of course also true of the conventional high-strain-rate pressure-shear test).

The normal velocity interferometer signal from this HSRPSR test is shown in Fig. 14 (time zero in this figure is identical to that in Fig. 12). The normal wave arrival is clearly evident, as is the arrival of the unloading wave from the flyer/balsa-wood rear surface. Both waves arrive at the times expected from the wave-propagating diagram of Fig. 8, after accounting for the slight delay induced by the

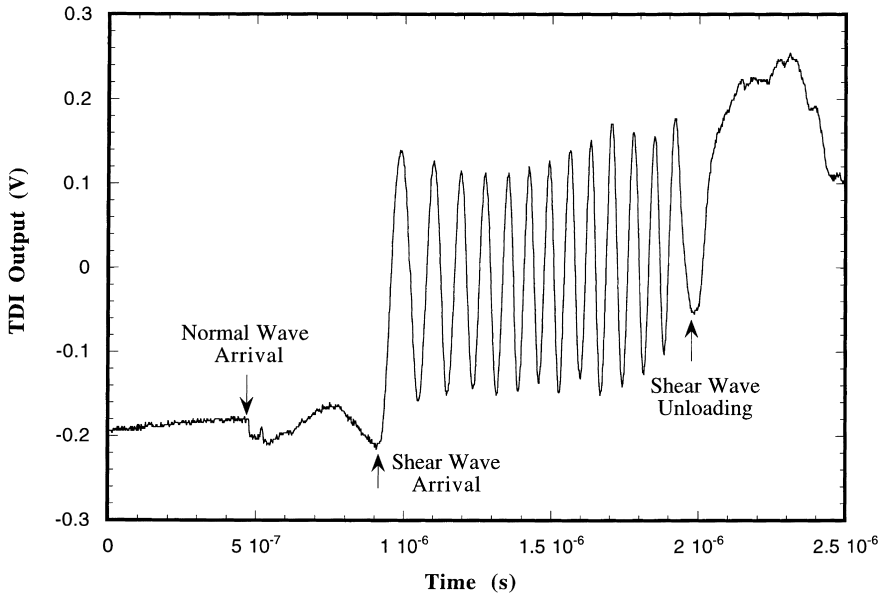

Fig. 12. Typical TDI signal from a HSRPSR experiment. The arrival times of the normal and shear waves are also shown. Each fringe in this signal corresponds to a transverse displacement of 2.5 μm.

inevitable tilt (the misalignment in this test was ~0.8 m rad). The wave arrivals indicate that the design parameters for this HSRPSR test are appropriate for ensuring that the specimen has been loaded in high-rate homogeneous shearing only once before the anvil/specimen interface separates. Closer inspection of the fringes corresponding to normal wave arrival in Fig. 14 actually reveals two normal wave arrivals about 66 ns apart. A very small gap between the thin specimen and the flyer plate results in an initial normal wave arrival due to contact between the specimen and anvil, followed shortly by a second normal wave arrival due to closure of the gap between the specimen and flyer. True material behavior is therefore not observed until after the gap closure. For this reason, the TDI signal is shifted by 66 ns (the gap closure time) so that the resulting shear stress vs shear strain curve reflects the true material response.

The critical question that remains is that of ensuring that the projectile has been brought to rest sufficiently quickly before imparting substantial additional momentum to the flyer/specimen assembly. The specimen in this experiment was found between the specimen holder and the catcher, and the foam 'witness plate' on the catcher showed no evidence indicating a collision with the specimen. Therefore, it can safely be concluded that the residual velocity of the specimen was very low (the catcher is about 0.3 m away from the specimen holder). Clearly a specimen that is only 120 μm thick is very easily bent, but the recovered specimen was almost flat with just a few scratches as shown in Fig. 15 (which compares the specimen obtained after the new HSRPSR test with a specimen obtained after a conventional high-strain-rate pressure-shear test at identical velocity and skew angle). The difference between the two specimens in Fig. 15 dramatically illustrates the value of the new recovery technique: it is obvious that microstructural characterization of the conventional pressure-shear specimen cannot be related solely to the homogeneous shearing sustained because of the initial loading.

The state of the flyer and anvil plates after the recovery test is shown in Fig. 16. It is observed that the anvil plate has broken into several pieces, while the flyer plate is almost completely intact except for two small chips near the periphery, also supporting the designed recovery mechanism. In summary, the

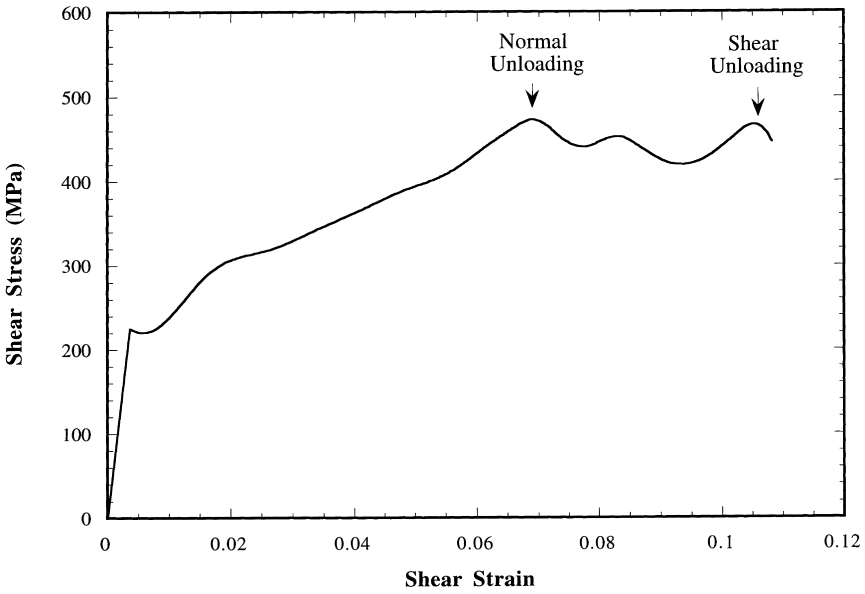

Fig. 13. Typical shear stress vs shear strain curve derived from the HSRPSR experiment of Fig. 12. The shearing signal may be affected by the tilted nature of the normal unloading wave. This stress–strain curve corresponds to a nominal strain rate of $0.91 \times 10^5\ s^{-1}$ and a superimposed compressive stress of 2.57 GPa.

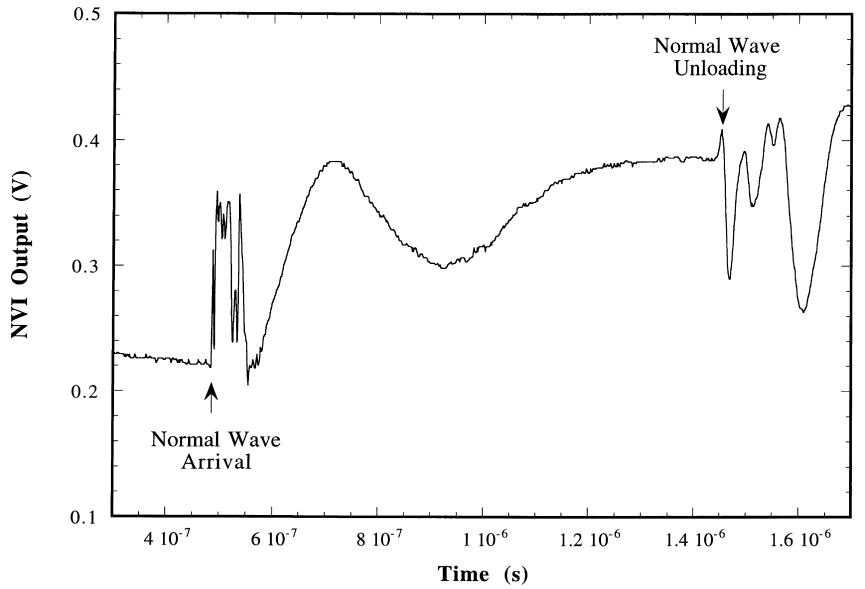

Fig. 14. Typical NVI signal from the HSRPSR experiment of Fig. 12. The arrivals of the normal loading and unloading waves occur at the times expected from the wave propagation diagram of Fig. 8

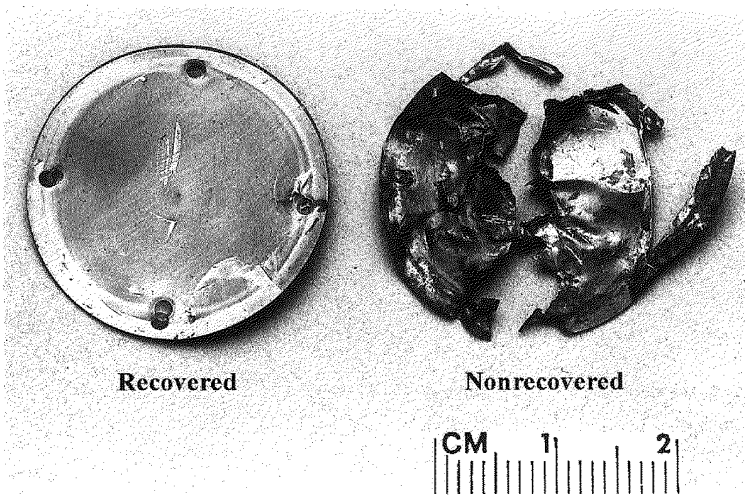

Fig. 15. Photograph comparing α-titanium specimens recovered using the HSRPSR technique and after a conventional high-strain-rate pressure-shear plate impact experiment at identical projectile velocity and skew angle. The specimen recovered after the HSRPSR experiment is clearly more suitable for the characterization of the microstructural mechanisms operational at these rates of deformation. (Scale is cm.)

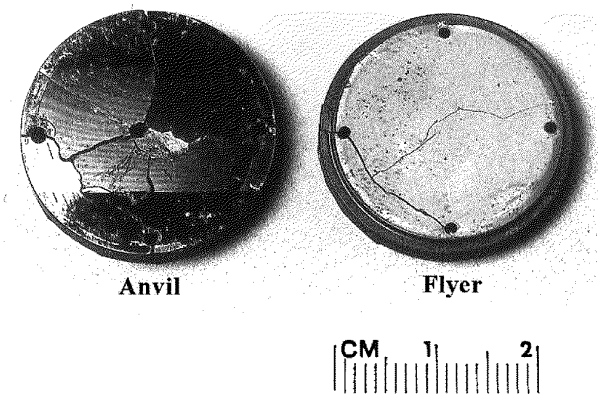

Fig. 16. Photograph of the flyer and anvil plate after the recovery experiment. The anvil plate acts as a momentum trap and is captured by the foam witness plate in the catcher; it is therefore much more damaged than the flyer plate, which has a very small residual velocity after the impact. (Scale is cm.)

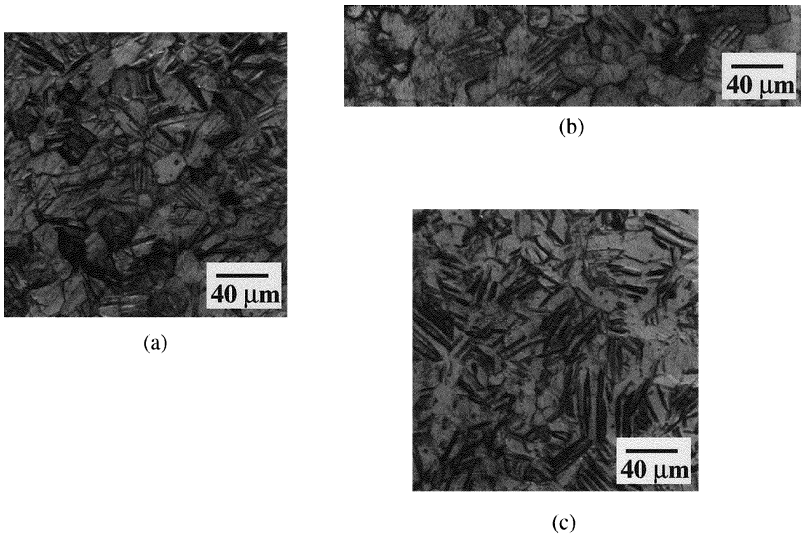

Fig. 17. Microstructure of an α-Ti specimen deformed in a high-strain-rate pressure-shear recovery experiment (a) transverse to the compression axis and (b) along the compression axis. The nominal shear rate was $1.04 \times 10^5\ s^{-1}$ and the superimposed compressive stress was 2.45 GPa. (c) Microstructure (transverse to compression axis) of an α-titanium specimen deformed using a compression Kolsky bar to the same effective strain as (a) at a strain rate of $3 \times 10^3\ s^{-1}$.

experimental observations indicate that both the wave propagation control for recovery and the momentum transfer mechanism designed for the new technique appear to function as desired, with only a very small residual velocity for the specimen and flyer. The magnitude of this residual velocity decreases with decreasing gap between the shoulder of the wedge and the front surface of the steel plate attached to the stopper. A gap of about 0.5 mm, as measured by a feeler guage, is found to be appropriate. The stopper assembly has been used successfully for projectile velocities of 70–200 ms^{-1}. The 3 mm thick steel plate glued to the front surface of the crosspiece is deformed plastically in the area around the hole after each test (see Fig. 11) and must be replaced, but the stopper frame has not exhibited any perceptible permanent deformation to date.

4.4. Microstructural characterization of recovered titanium specimens

A peculiar difficulty associated with identification of the relative importance of deformation mechanisms within h.c.p. metals like α-titanium arises from the fact that these crystal structures may undergo both slip and twinning during plastic deformation. There are therefore two major components to the microstructural evolution that are of interest, the first associated with dislocation substructure and the second associated with deformation twinning. A complete description of the evolution of dislocation substructure and deformation twinning with strain rate in α-titanium is presented by Chichili et al. (1997) using specimens recovered in compression Kolsky bar experiments. At the microscopic level, these authors observed macrotwins in the optical microscope and microtwins in the TEM; the twins were of $\{10\bar{1}2\}$ type with secondary twinning occurring at large plastic strains and high strain rates. The density of these twins increased with both strain and strain rate, and was shown to be a unique function of the compressive flow stress for all of the strain rates and all of the strains at which the microstructural measurements were made.

One of the α-titanium specimens recovered after a HSRPSR experiment was sectioned for microstructural examination, and an optical micrograph of the deformed structure is shown in Fig. 17(a) and (b). The material is obviously heavily twinned, but it appears that the twin density is not as high as observed in compression Kolsky bar experiments (the microstructure of an α-titanium specimen deformed at a strain rate of 3×10^3 s^{-1} is presented in Fig. 17(c). This is unexpected, since the flow stresses developed in the pressure-shear experiments described in this paper are considerably higher than those developed at compression Kolsky bar rates, and in light of the results of Chichili et al., 1997. It is possible that the superimposed hydrostatic pressure has constrained the development of deformation twins. It is also possible that shear stresses alone do not cause significant deformation twinning in polycrystalline α-titanium (little twinning was observed by Chichili (1997) in high-rate torsional Kolsky bar tests). These important microstructural evolution observations are only possible because of the new high-strain-rate pressure-shear recovery technique.

An interesting secondary observation that can be made from the through-thickness micrograph of Fig. 17(b) is that the deformation was clearly macroscopically homogeneous, i.e. no shear bands are observed within the plate impact specimens. Grebe et al. (1985) observed intense shear localization in α-titanium when subjected to impact loading at velocities ranging from 600–800 ms^{-1} and Kobayashi (1987) observed shear localization in CP titanium at a critical strain of 50% (note that the total local strains achieved in the tests of Grebe et al. (1985) were also very high). Since the total strains achieved in the plate impact experiments described here are only of the order of 10%, shear bands should not be expected within this plate impact specimen and indeed none are observed.

5. Discussion

The new experimental technique, while slightly more complex than the conventional high-strain-rate pressure-shear experiment, is able to provide the same high-strain-rate constitutive response and in addition allows for the evaluation of microstructural evolution within materials at very high strain rates. This new capability will not only be useful for the development of improved, more mechanism-based constitutive equations, but should lead to a much clearer understanding of the dependence of these deformation mechanisms on the multiaxial stress states that can be attained through pressure-shear. This latter application is clearly evidenced in the results presented on α-titanium here. Several potential applications of the new technique are currently being pursued in this laboratory.

The new pressure-shear recovery technique can also be compared with the single-wave pressure-shear recovery approach of Yadav et al. (1993) and Machcha and Nemat-Nasser (1994). The two pressure-shear recovery techniques have two very different objectives and so different sets of applications. Both SWPSR and HSRPSR experiments require the projectile to be stopped immediately after impact and both rely on a momentum trap to carry away the entire compression loading pulse. The fundamental difference lies in the fact that in the high rate configuration (HSRPSR) it is not necessary to trap the entire shear loading pulse in the momentum trap. Because the specimen is very thin, only a very small fraction of the shear loading pulse remains in the specimen itself and causes negligible additional deformation because the two specimen surfaces are quickly unloaded and are very close together. The shear waves remaining in the flyer plate also cannot reload the specimen because there is no longer a compressive stress to couple the flyer and specimen surfaces. These features greatly simplify the HSRPSR technique. However, the substantial standoff created by the stopper assembly makes the pre-test alignment procedure considerably more difficult.

6. Summary

The following points summarize this work:

- A new experimental technique, called the High-Strain-Rate Pressure-Shear Recovery or HSRPSR technique, has been developed for the recovery of specimens that have been subjected to a well-characterized homogeneous high-rate shearing deformation at strain rates on the order of 10^5 s^{-1}.
- The new technique provides all of the primary attributes of the conventional high-strain-rate pressure-shear experiment, while extending that technique to allow the determination of high-rate deformation mechanisms within materials.
- This new pressure-shear recovery technique has proven successful in the recovery of α-titanium thin specimens, and shear stress vs shear strain curves have been obtained at a strain rate of $\sim 10^5$ s^{-1}.
- The development of deformation twins in α-titanium at high strain rates appears to be a strong function of not only the magnitude of the applied stress but also the multiaxial nature of the stress state.

Acknowledgements

The authors would like to acknowledge the support of the U.S. Army Research Office through Grant Nos. DAAL03-91-G-0079 and DAAH04-95-I-0417, and of the National Science Foundation through Grant No. CMS-9402618.

References

Chichili, D.R., 1997. High-strain-rate deformation mechanisms and adiabatic shear localization in alpha-titanium. Ph.D. Dissertation, The Johns Hopkins University.

Chichili, D.R., Ramesh, K.T., 1995. Dynamic failure mechanisms in a 6061-T6 Al/Al_2O_3 metal-matrix composite. International Journal of Solids and Structures 32 (17/18), 2609–2626.

Chichili, D.R., Ramesh, K.T., Hemker, K.J., 1998. The high-strain-rate response of alpha-titanium: experiments, deformation mechanisms, and modeling. Acta Materialia 46 (3), 1025–1043.

Clifton, R.J., Klopp, R.W., 1980. Pressure-shear plate impact testing. ASM Metals Handbook, vol. 8. ASM International, OH, p. 230.

da Silva, M.G., Ramesh, K.T., 1997. The rate-dependent deformations of porous pure iron. International Journal of Plasticity 13 (6–7), 587–610.

Duffy, J., Campbell, J.D., Hawley, R.H., 1971. On the use of a torsional split Hopkinson bar to study rate effects in 1100-0 aluminum. Trans. ASME: J. Appl. Mech 38, 83–91.

Follansbee, P.S., Gray, G.T., 1989. An analysis of the low temperature, low and high strain-rate deformation of Ti-6Al-4V. Metall. Trans. A 20A, 863.

Grebe, H.A., Pak, H., Meyers, M.A., 1985. Adiabatic shear localization in titanium and Ti-6 Pct Al-4 Pct V alloy. Metall. Trans. A 16A, 761.

Kim, K.S., Clifton, R.J., 1977. A combined normal- and transverse-displacement interferometer with an application to impact of y-cut quartz. Journal of Applied Physics 48, 4132.

Kobayashi, H., 1987. Shear localization and fracture in torsion of metals. Ph.D. Thesis, University of Reading.

Kolsky, H., 1949. An investigation of the mechanical properties of materials at very high rates of loading. Proc. Phys. Society, 62B, p. 676.

Kumar, P., Clifton, R.J., 1979. Dislocation motion and generation in LiF crystals subjected to plate impact. Journal of Applied Physics 50, 4747.

Machcha, A.R., Nemat-Nasser, S., 1994. Pressure-shear recovery experiments. Mechanics of Materials 18, 49.

Mecking, H., Kocks, U.F., 1981. Kinetics of flow and strain-hardening. Acta Metall. Mater. 29, 1865.

Nemat-Nasser, S., Isaacs, J.B., Starrett, J.E., 1991. Hopkinson techniques for dynamic recovery experiments. Proc. R. Soc. Lond. A, 435, p. 371.

Ramesh, K.T., Kelkar, N., 1995. Technique for the continuous measurement of the projectile velocity in plate impact experiments. Rev. Sci. Instrum. 66, 3034.

Ramesh, K.T., Clifton, R.J., 1992. Finite deformation analysis of pressure-shear plate impact experiments on elastohydrodynamic lubricants. Journal of Applied Mechanics 59 (4), 754–761.

Yadav, S., Ramesh, K.T., 1995. The mechanical properties of tungsten-based composites at very high strain rates. Materials Science & Engineering A 203, 140–153.

Yadav, S., Chichili, D.R., Ramesh, K.T., 1995. The mechanical properties of a 6061-T6 Al/Al_2O_3 metal-matrix composite at high rates of deformation. Acta Metallurgica 43 (12), 4453–4464.

Yadav, S., Davis, J.A., Ramesh, K.T., 1993. Damage and recovery experiments using pressure-shear plate impact. In: Ramesh, K.T. (Ed.), Experimental Techniques in the Dynamics of Deformable Solids, ASME AMD, vol. 165, pp. 71–78.

Yoo, M.H., 1981. Slip, twinning, and fracture in hexagonal close-packed metals. Metall. Trans. A 12A, 409.

Zerilli, P.J., Armstrong, R.W., 1987. Dislocation-mechanics-based constitutive relations for material dynamic calculations. Journal of Applied Physics 61, 1816.